Local Buckling of RBS Beams Subjected to Cyclic Loading

Feng-Xiang Li[1]; Iori Kanao[2]; Jun Li[3]; and Kiyotaka Morisako[4]

Abstract: This paper presents an analytical study of local instability behavior in a reduced beam section (RBS) beam subjected to cyclic loading. A general finite-element method is used for numerical experiments here. Even though lateral instability in the RBS beam is prevented, strength deterioration may occur due to local buckling of the RBS portion. The writers suggest that stiffeners arranged in the RBS portion can delay the occurrence of local buckling. To address the possibility that reinforcement of the RBS portion might offset the advantage of RBS, the stress distribution of beam end of the RBS with stiffeners was compared to that of an RBS beam without stiffeners. Stiffening the RBS portion did not cause an excessive stress concentration. These analyses suggest that an RBS beam can be sufficiently strengthened by placing two stiffeners at the boundaries that divide the RBS portion into three equal regions and the stiffener thickness required is the same thickness as the web.

DOI: 10.1061/(ASCE)ST.1943-541X.0000073

CE Database subject headings: Beams; Cyclic loads; Buckling; Stiffening; Postbuckling.

Introduction

The 1994 Northridge and 1995 Hyogoken-Nanbu earthquakes caused serious damage to steel structures. In particular, brittle fracture in welded beam-column connections hindered reconstruction after the earthquakes. Therefore, many studies of connection details have been conducted in both the United States and Japan and various details have been proposed for ensuring beam plastic rotation capacity sufficient to endure large earthquake motions. In the United States, new strengthened details near the beam-column connections have been proposed to reduce damage to the connections. A welded haunch scheme exhibited sufficient plastic rotation capacity in experiments and numerical simulations (Engelhardt et al. 1998; Uang et al. 2000; Yu et al. 2000; Lee and Uang 2001). This detail requires more steel plates and more welding parts.

An innovative detail known as reduced beam section (RBS) has been also proposed and investigated extensively. The RBS detail has proven sufficient in providing beam plastic rotation capacity by many experimental studies [for example, Engelhardt and Sabol (1997); Engelhardt and Sabol (1998); Uang and Fan (2001); Chi and Uang (2002); Jones et al. (2002); Lee et al. (2005)]. The RBS detail can be produced without special machining skills and it has been used practically. The lateral bracing requirements for RBS beams to prevent lateral buckling may be the same as the requirements for standard beam (Nakashima et al. 2002).

However, in RBS beams, strength deterioration caused by local instability has not yet been examined and it is worthwhile to evaluate the local instability of these beams. This paper presents an analytical study of local buckling, postbuckling behavior, and the effects of stiffeners in RBS beams subjected to cyclic loading.

Verification of Numerical Analysis

A general finite-element method (FEM) program code, MSC-.MARC 2005, was used in this study. The accuracy of the FEM predictions of significant local buckling was assessed by comparing the FEM results to a physical test of a full-scale beam-column subassemblage (Engelhardt et al. 1998). The subassemblage was T-shaped and consisted of a beam and column, as shown in Fig. 1(a). The column ends were simple supported. The specimen was constructed from a W36×150 beam and a W14×426 column. The beam was loaded cyclically with increasing beam chord angle amplitudes of 0.003 7, 0.005 6, 0.007 5, 0.015, 0.022 4, 0.03, and 0.037 rad. Three cycles were performed for the 0.003 7,

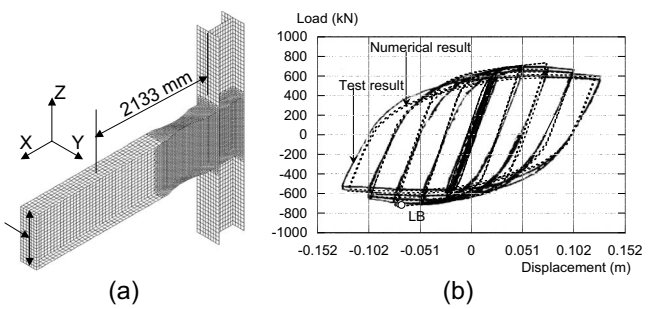

Fig. 1. Comparison of the FEM and physical test results for a full-scale RBS beam-column subassemblage: (a) beam-column model; (b) relationship between tip load and tip displacement

[1]Doctoral Student, Graduate School of Science and Technology, Kyoto Institute of Technology, Matsugasaki, Sakyo-ku, Kyoto 6068585, Japan (corresponding author). E-mail: reihouka@gmail.com

[2]Associate Professor, Graduate School of Science and Technology, Kyoto Institute of Technology, Matsugasaki, Sakyo-ku, Kyoto 6068585, Japan.

[3]Associate Professor, School of Civil Engineering, Qingdao Technological Univ., 11 Fushun Rd., Qingdao 266033, People's Republic of China.

[4]Professor, Graduate School of Science and Technology, Kyoto Institute of Technology, Matsugasaki, Sakyo-ku, Kyoto 6068585, Japan.

Note. This manuscript was submitted on December 12, 2007; approved on May 4, 2009; published online on May 6, 2009. Discussion period open until May 1, 2010; separate discussions must be submitted for individual papers. This paper is part of the ***Journal of Structural Engineering***, Vol. 135, No. 12, December 1, 2009. ©ASCE, ISSN 0733-9445/2009/12-1491–1498/$25.00.

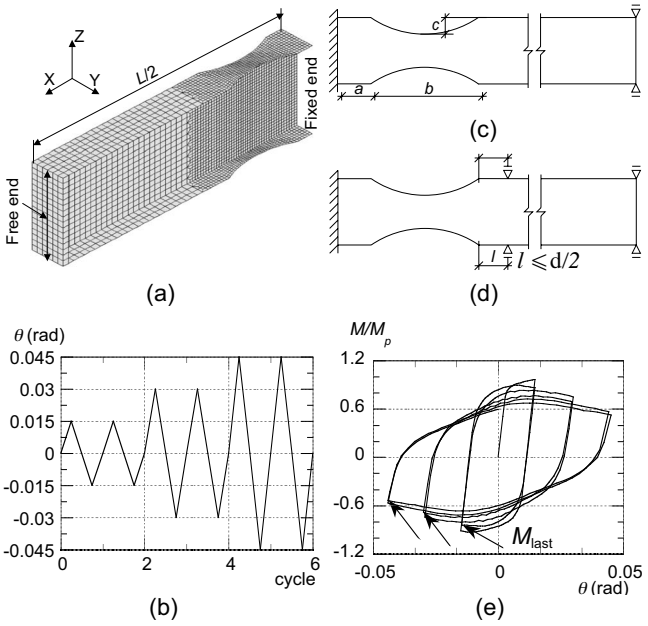

Fig. 2. Beam modeling: (a) cantilever representation and discretization; (b) loading history; (c) details of the RBS portion; (d) details of the RBS beam with supplemental lateral bracings; and (e) definition of the strength measurement

0.005 6, 0.007 5, 0.015, and 0.022 4-rad amplitudes and two cycles were performed for the 0.03 and 0.037-rad amplitudes.

In the analysis, four-node thick-shell elements were used with a size of 25 mm × 25 mm in regions where large plastification was expected. The FEM model of the beam-column subassemblage is shown in Fig. 1(a). Since the column base was pin supported, the rotation angle about the X and Z axes and the vertical and horizontal displacements were fixed for the numerical analyses. For the roller-supported column top, the horizontal displacement and the rotation angle about X and Z axes were fixed, as was the Y-displacement of the beam tip. The lateral bracing was placed at 2,133 mm from the column face in the test and the Y-displacement at this location was also fixed. The loading history used in the model was the same as the load patterns applied to the beam-column assemblage. A bilinear stress-strain relation was used, with the second stiffness equal to 1/100 of the initial Young's modulus (E). The Young's modulus and the yield stress of the material were 210 and 285 MPa, respectively.

The test result (solid line) is compared with the FEM analytical result (dotted line) in Fig. 1(b), which shows the beam tip load versus displacement. The experimental and analytical behaviors, including strength deterioration due to local buckling (Engelhardt 1999), agreed well. In the FEM analysis, local buckling occurred during the 0.022 4-rad cycle (76 mm). The FEM program code had sufficient numerical precision to compute this accurately.

Table 1. Properties of Beams with Varying Cross Sections

	W24 × 76	W30 × 99	W36 × 194
I_y (mm^4)	8.5×10^8	16.2×10^8	49.6×10^8
r_y (mm)	48.91	53.66	65.80
L (mm)	3580	3928	4816
Width-thickness ratio	52.2	55.3	45.4
a (mm)	114	132	154
b (mm)	494	621	773
c (mm)	57	66	77

Local Buckling of Reduced Beam Section Beams Subjected to Cyclic Loading

Analysis Model

The effect of local instability on deformation capacity was analyzed using the previously verified FEM model. The analysis model is shown in Fig. 2(a). The beam is modeled as a cantilever beam of half-span length ($L/2$) with a concentric force applied at the free end. This is the simplest model for investigating the influence of local buckling in RBS beams. Four-node thick-shell elements were used and the end portion that could sustain plastic deformation was 25 mm × 25 mm. The stress-strain relation followed a bilinear model in which the second stiffness was $E/100$ and the yield stress was 235 MPa. The analysis was repeated with a yield stress of 345 MPa.

All displacements and rotation were restrained at the fixed end. At the free end, the Y-displacement and warping were restrained. The loading history is shown in Fig. 2(b). The beam was loaded cyclically with increasing beam chord angle amplitudes of 0.015, 0.030, and 0.045 rad (Nakashima et al. 2002). Each loading process was repeated twice.

The beam cross sections adopted in this study were W24 × 76, W30 × 99, and W36 × 194. The physical properties of these beams are shown in Table 1. A detailed schematic of the RBS portion of the beams is shown in Fig. 2(c) and the dimensions are given in Table 1. The design of the RBS beams followed the guidelines proposed by Engelhardt (1999). According to

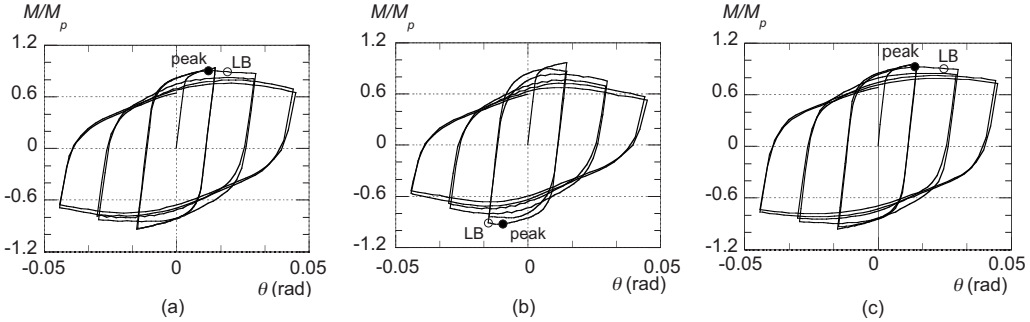

Fig. 3. Relationship between end moment and end rotation in the standard RBS beams (STF-0) with three cross sections: (a) W24 × 76; (b) W30 × 99; and (c) W36 × 194

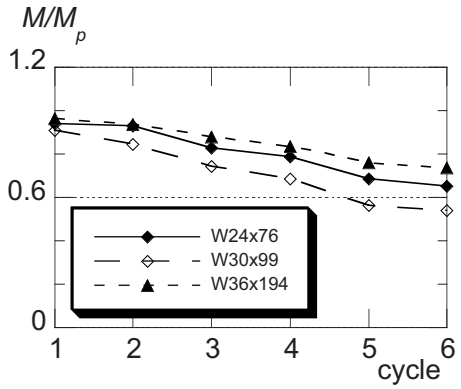

Fig. 4. Relationship between last strength and loading cycles in the standard RBS beams with three cross sections

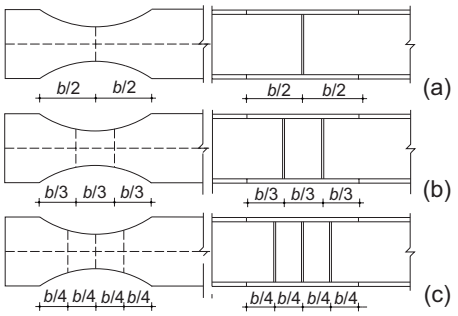

Fig. 6. Placement of stiffeners in RBS beams with (a) one stiffener (STF-1); (b) two stiffeners (STF-2); and (c) three stiffeners (STF-3)

ANSI/AISC 341-05 (AISC 2005a), the length (L) of an RBS beam should be less than $77r_y$, where r_y is the radius of gyration with respect to the weak axis of the beam. The slenderness ratio (L/r_y) of the three beams used here was 73.2.

Nakashima et al. (2002) suggested that RBS beams should be less susceptible to lateral-torsional buckling than standard beams with the same nominal slenderness ratio and therefore the lateral bracing requirements stipulated for standard beams should also be sufficient for RBS beams. According to ANSI/AISC 358-05 (AISC 2005b), RBS beams require supplemental lateral bracings, which are located $0.5d$ beyond the end of the RBS farthest from the face of the column [Fig. 2(d)].

The strength at the maximum amplitude of each cycle is adopted as the strength measure in the following examination [see Fig. 2(e)]. This strength is named "last strength" here.

The results of modeling the beam with a yield stress of 345 MPa were similar to those from modeling with a yield stress of 235 MPa so all of the results presented are for the 235-MPa analyses.

Local Instability

Figs. 3(a–c) show the relationship between the beam-end moment (M) and the beam-end rotation obtained for the W24×76, W30×99, and W36×194 cross sections. The beam-end moment was normalized to the full plastic moment (M_p) for the full section. The beam-end moment was computed by multiplying the beam tip force by the distance to the beam end ($L/2$). In these figures, an open circle (○) indicates the local buckling point and a filled circle (●) indicates the peak point of the cycle in which local buckling occurred. In Fig. 3, the local buckling point is close to the peak point. No significant lateral buckling occurred up to the end of cyclic loading. However, even without lateral instability in the RBS beam, the strength may deteriorate due to local buckling.

Fig. 4 shows the relationship between the last strength and load cycles for standard RBS beams with the three analyzed cross sections. For the W24×76 and W36×194 beams, the last strengths of the sixth cycle (0.045-rad amplitude) deteriorated to about 30 and 20% of the maximum strength, respectively. The W30×99 beam exhibited greater strength deterioration, approximately 40% during the sixth cycle. Of the three analyzed cross sections, W30×99 has the largest web-width-to-thickness ratio of 55.3. When the width-thickness ratio is large, representing a cross section with a thinner web, the plasticity deformation capacity is more prone to deterioration due to local buckling.

Fig. 5 shows the relationship between end moment and beam-end rotation of RBS beams with supplemental lateral bracings for W24×76, W30×99, and W36×194 cross sections. For the W30×99 beam, local buckling occurred during the third cycle, while there was no obvious lateral buckling. Local buckling in RBS beams with sufficient lateral bracings may cause strength deterioration. Supplemental lateral bracings may be moderately effective at preventing lateral buckling but cannot prevent local buckling.

Deformation Capacity of RBS Beams with Stiffeners

Number of Stiffeners

Stiffeners were placed in the RBS portion of the beam to prevent strength deterioration caused by local buckling. The stiffeners

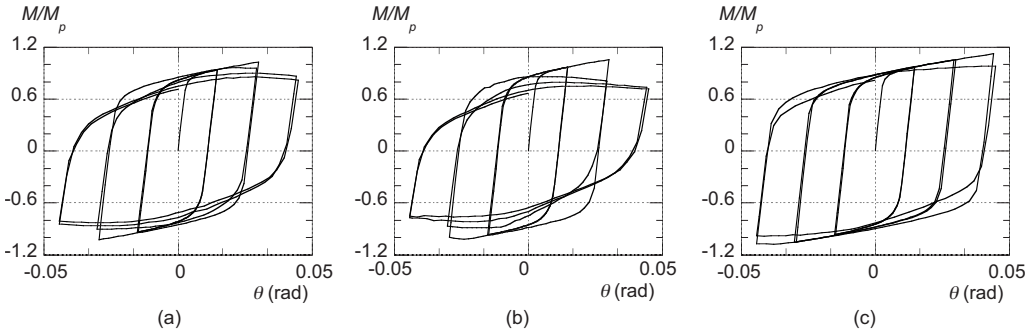

Fig. 5. Relationship between end moment and end rotation in three RBS beams with supplemental lateral bracings: (a) W24×76; (b) W30×99; and (c) W36×194

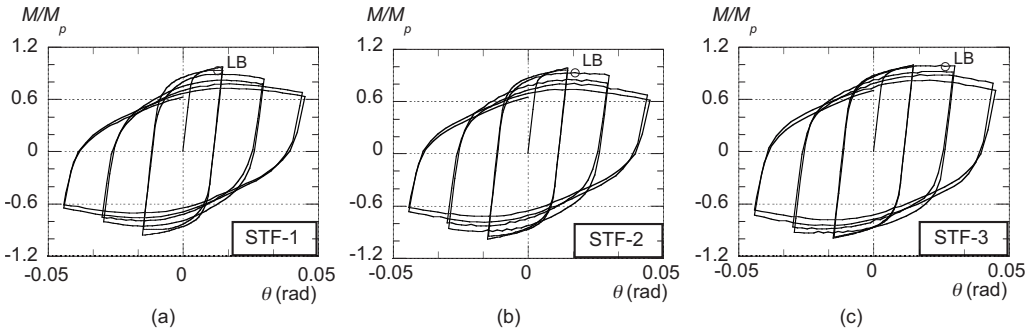

Fig. 7. Relationship between end moment and end rotation in W30×99 beams with stiffeners: (a) STF-1; (b) STF-2; and (c) STF-3

were the same thickness as the web. As shown in Fig. 6, three types of stiffener arrangements were adopted here. STF-1 has one pair of stiffeners in the center of the RBS portion. STF-2 has two pairs of stiffeners arranged at the boundaries that divide the RBS portion into three equal regions. STF-3 has three pairs of stiffeners arranged at the boundaries that divide the RBS portion into four equal regions. The RBS beam with no stiffener is named STF-0.

Fig. 7 shows the relationship between beam-end moment and end rotation obtained from the W30×99 RBS beams with stiffeners. A comparison of Fig. 7(a) with Fig. 3(b) shows that adding stiffeners delays local buckling. The occurrence of local buckling differs significantly between the standard RBS beam (STF-0) and the RBS beams with stiffeners. For STF-0 and STF-1, local buckling occurs during the first and second cycles (0.015-rad amplitude), respectively. For STF-2 and STF-3, local buckling occurs during the third cycle (0.030-rad amplitude). A comparison of Fig. 7(b) with Fig. 5(b) indicates that the RBS beam with two pairs of stiffeners has almost the same strength as the standard RBS beam with supplemental lateral bracings.

Fig. 8 shows the relationship between the last strength and load cycles for the standard RBS beam and the RBS beams with stiffeners. The last strengths of the RBS beams with stiffeners are significantly higher than the last strength of STF-0. For the W24×76 beams, the last strength of STF-0 is less than $0.8M_p$ after the fourth cycle (0.030-rad amplitude). However, the last strengths of STF-1 and STF-2 are greater than $0.8M_p$ until the fifth cycle. The last strength of STF-3 is greater than $0.8M_p$ during the entire loading history. For the W30×99 beams, the last strength of STF-0 is less than $0.8M_p$ after the third cycle (0.030-rad amplitude). The last strength of STF-1 is greater than $0.8M_p$ until the third cycle while the last strengths of STF-2 and STF-3 exceed $0.8M_p$ until the fourth cycle. For the W36×194 beams,

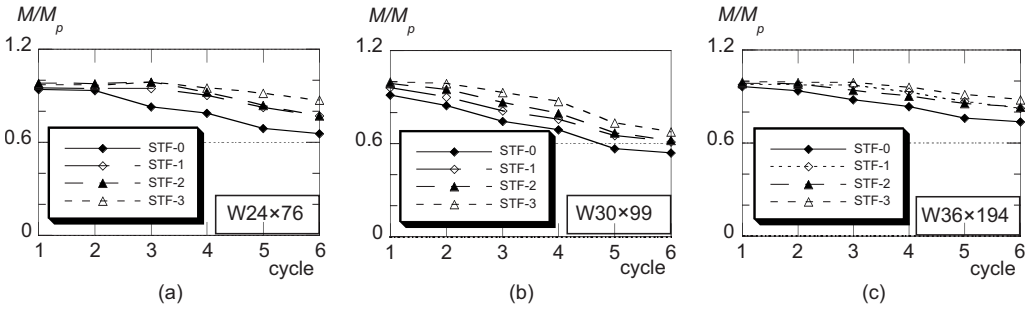

Fig. 8. Relationship between last strength and load cycles in RBS beams, both with and without stiffeners, with three cross sections: (a) W24×76; (b) W30×99; and (c) W36×194

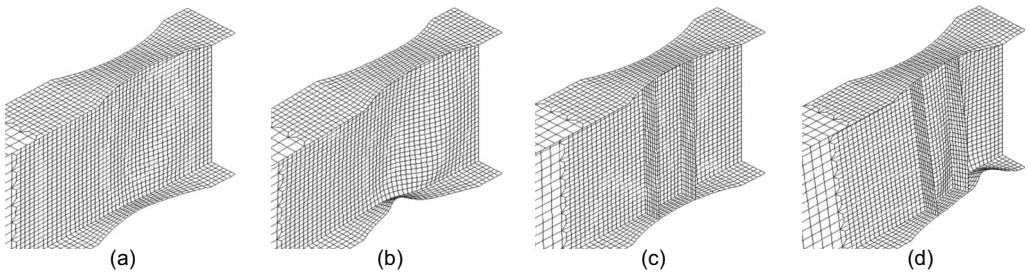

Fig. 9. Local deformations at the RBS portion of the W30×99 beam: (a) deformation of STF-0 at the maximum negative amplitude of the second cycle; (b) deformation of STF-0 at the maximum negative amplitude of the sixth cycle; (c) deformation of STF-2 at the maximum negative amplitude of the second cycle; and (d) deformation of STF-2 at the maximum negative amplitude of the sixth cycle

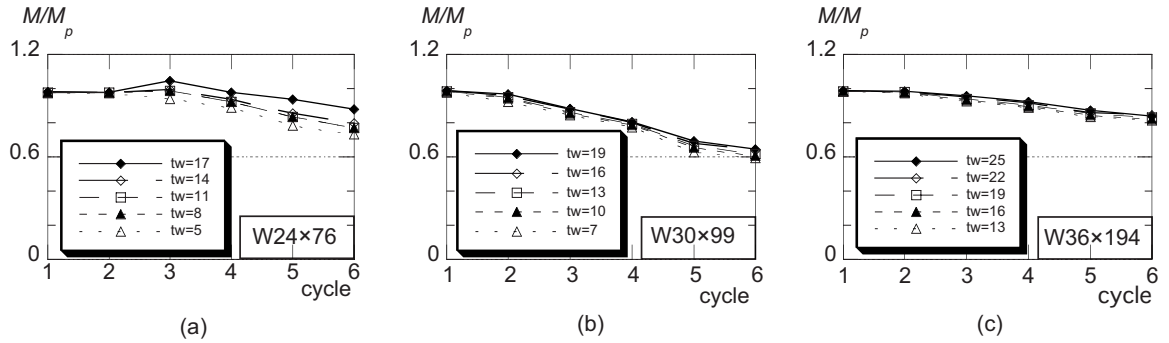

Fig. 10. Relationship between last strength and load cycles in RBS beams with stiffeners of varying thickness. The beams have three different cross sections: (a) W24×76; (b) W30×99; and (c) W36×194.

the last strength of STF-0 is less than $0.8M_p$ after the fifth cycle (0.045-rad amplitude) but the last strengths of STF-1, STF-2, and STF-3 exceed $0.8M_p$ for all cycles.

As these results show, stiffeners can delay local buckling and can also improve strength deterioration. The minimum interstory drift angle required for an intermediate moment frame is 0.020 rad [ANSI/AISC 341-05 (AISC 2005a,b), FEMA-350 (FEMA 2000)]. Therefore, two pairs of stiffeners are required in the RBS portion until the maximum deformation angle is 0.030 rad. The maximum strength of the beam with stiffeners is less than the full plastic moment (i.e., $M/M_p < 1.0$).

Fig. 9 illustrates selected deformation states of the W30×99 beams. Figs. 9(a and b) show STF-0 at the maximum negative amplitude of the second and sixth cycles, respectively. Figs. 9(c and d) show STF-2 at the same points. The most intense local buckling was observed in STF-0. At the second cycle, local buckling occurred in STF-0. At the sixth cycle, the deformation of STF-2 was smaller than that of STF-0.

Thickness

The influence of stiffener thickness was evaluated in STF-2. Fig. 10 shows the relationship between the last strength and load cycles for various stiffener thicknesses. Here, an open square (□) represents a stiffener thickness equal to the web thickness while the diamonds (◆ and ◇) indicate stiffeners thicker than the web and the triangles (▲ and △) denote stiffeners thinner than the web. Except for the filled diamond (◆) in Fig. 10(a), the last strengths are approximately the same. The stiffener thickness only minimally influences the last strength of the RBS beams under cyclic loading. Therefore, a stiffener thickness equal to the thickness of web is sufficient.

Placement

The stiffeners in STF-2 and STF-3 were placed such that they divided the RBS portion into three or four equal parts, respectively. An alternative arrangement is to place the stiffeners at both ends of the RBS portion, as shown in Fig. 11. This is referred to as STF-2-2. Similarly, in STF-3-2, the three pairs of stiffeners were located at the ends and the center of the RBS portion. Fig. 12 shows the relationship between the last strength and load cycles for the W24×76, W30×99, and W36×194 beams. Figs. 12(a–c) demonstrate that the last strength of STF-2 is larger than that of STF-2-2 for all three cross sections. Figs. 12(d–f) show that the last strength of STF-3 is equal to or slightly greater than that of STF-3-2. From these results, it is clear that placing the stiffeners equidistant from each other in the RBS portion strengthens the beam more than placing the stiffeners at each end of the RBS portion.

Stress Concentration

The stiffeners in the RBS portion improve the last strength under cyclic loading but the advantages of RBS beams may be lost. Therefore, the stress states of the fixed end and the central part of the RBS portion were examined. Fig. 13 shows the von Mises stress of the W24×76 beam at the fixed end and at the center of the RBS portion at the maximum negative amplitude of the sixth cycle. The stress was normalized by the yield stress. The upper flange was under tension and the lower flange was compressed. Figs. 13(a and b) illustrate the stress distribution of the upper flange of the fixed end and the RBS portion, respectively. The change in stress is very small. Fig. 13(c) shows the stress distribution of the lower flange of the fixed end of the beam. The stress of the RBS beams with stiffeners is slightly smaller than the yield stress (σ_y) but the maximum stress ratio (σ/σ_y) of STF-3 is 1.25. Fig. 13(d) presents the stress distribution in the lower flange of the central RBS portion. For STF-0, the maximum stress occurs in the middle of the central RBS portion. In contrast, for the RBS beams with stiffeners, the maximum stress occurs at the edge of the flange. The maximum stress ratio of STF-0 is about 1.6. The maximum stress ratio of STF-2 is 2.0 and it is nearly 25% larger than the standard RBS beam.

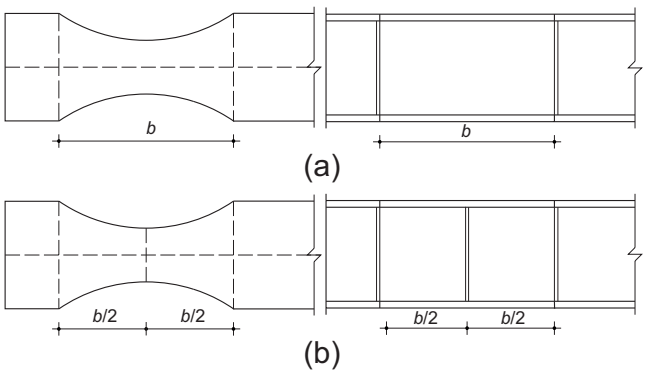

Fig. 11. Stiffeners' location in the RBS portion: (a) two stiffeners—one on each side of the RBS region (STF-2-2); (b) three stiffeners—one on each side of the RBS region and one in the middle (STF-3-2)

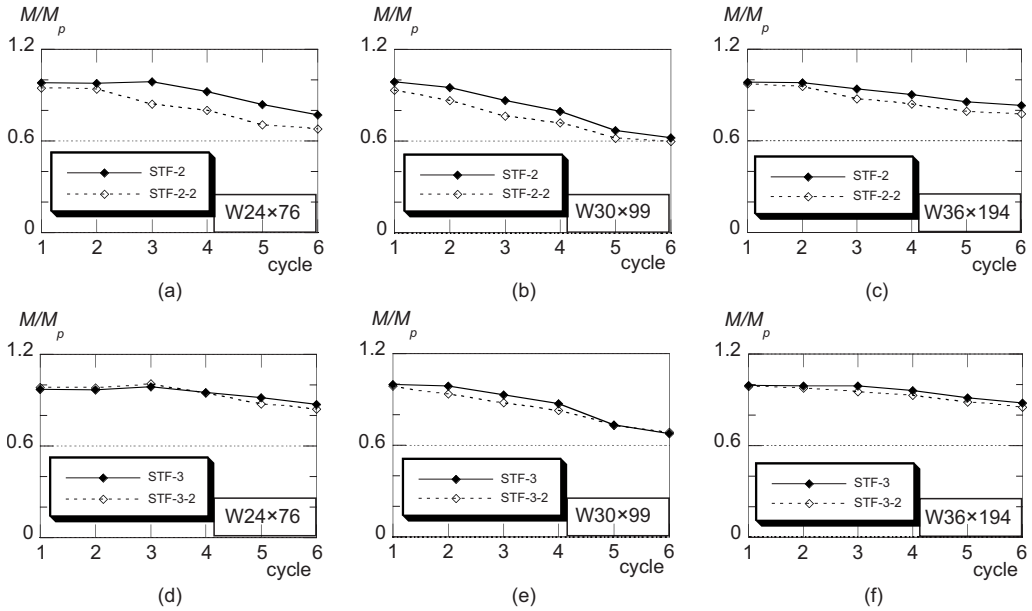

Fig. 12. Relationship between last strength and load cycles in RBS beams with stiffeners: a comparison of STF-2 and STF-2-2 for the (a) W24×76; (b) W30×99; and (c) W36×194 beams; a comparison between STF-3 and STF-3-2 for the (d) W24×76; (e) W30×99; and (f) W36×194 beams

Table 2 lists the maximum stress at the maximum displacement obtained from each cross section during the sixth cycle at the fixed end and the RBS portion of the beam. The stress was normalized by the yield stress. In the center of RBS portion, the stress ratios of STF-2 and STF-3 grew to about 2.0, which indicates that there may have been cracks in the flange of the RBS beams with stiffeners. The maximum stress at the fixed end of the RBS beams with stiffeners was almost the same as the maximum stress of standard RBS beams.

Fig. 14 shows the stress histories of STF-2 and STF-3 with a cross section of W24×76 at the monitoring point in Fig. 14(c). Up to 0.030 rad of amplitude, the stress ratio was maintained at 1.7. At 0.045 rad, the maximum stress ratio of STF-2 is larger than 2.0. Up to 0.030 rad of beam rotation angle, the stress concentration caused by stiffeners can be neglected.

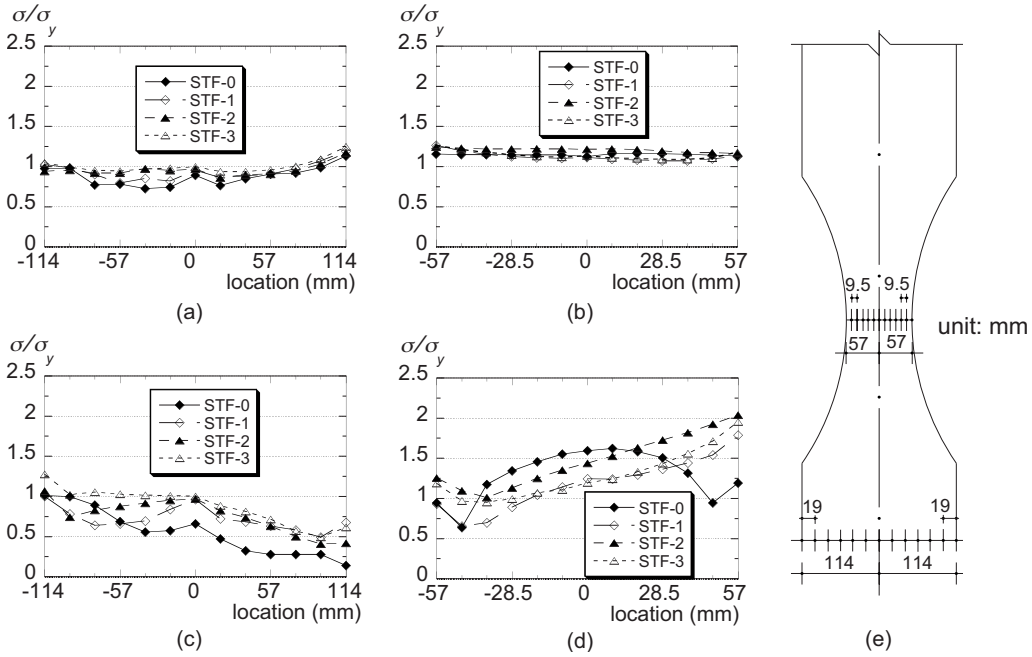

Fig. 13. Comparison of stress distribution in standard and stiffened W24×76 RBS beams with the end rotation at the maximum negative amplitude of the sixth cycle: (a) upper flange of the fixed end; (b) upper flange of the RBS portion; (c) lower flange of the fixed end; (d) lower flange of the RBS portion; and (e) stress monitoring points

Table 2. Maximum Stress at the Maximum Displacement of the RBS Beams during the Sixth Cycle

		σ/σ_y					
		STF-0	STF-1	STF-2	STF-3	STF-2-2	STF-3-2
W24×76	Fixed end	1.133	1.187	1.198	1.379	1.028	1.074
	RBS section	1.637	1.787	2.056	1.960	1.712	1.772
W30×99	Fixed end	1.121	1.136	1.116	1.145	1.028	1.038
	RBS section	1.602	1.567	1.831	1.744	1.755	1.553
W36×194	Fixed end	1.148	1.092	1.346	1.526	1.043	1.063
	RBS section	1.780	1.817	2.074	1.685	1.714	1.754

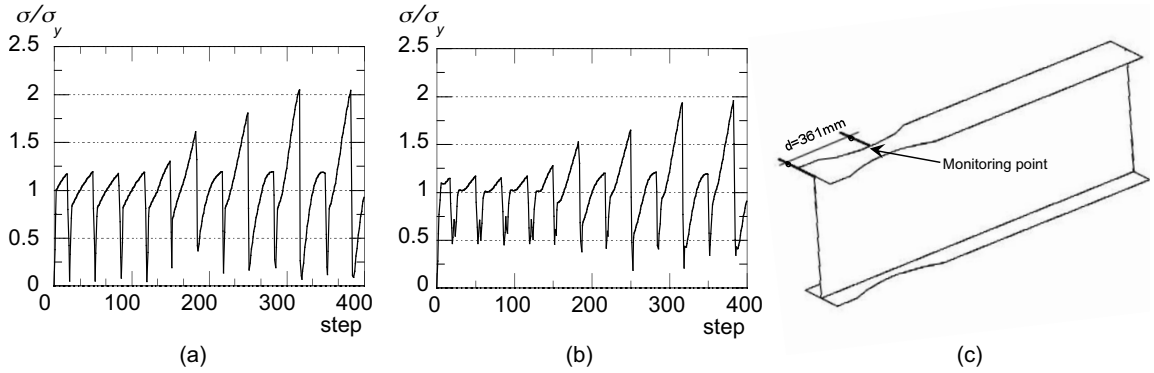

Fig. 14. Stress history at the upper flange of the RBS beams with stiffeners: (a) STF-2; (b) STF-3; and (c) stress monitoring point

Conclusions

This paper presents an analytical study of local instability and the effect of stiffeners on RBS beams subjected to cyclic loading. The major findings obtained from this study are summarized as follows:

1. There is no significant lateral buckling in RBS beams with an unbraced length of $73.2r_y$. However, strength deterioration caused by local buckling did occur under cyclic loading. This suggests that local buckling causes strength deterioration even when the lateral buckling is minimized.
2. Stiffeners placed in the RBS portion of the beam can effectively delay local buckling and increase beam strength. For the W36×194 beams, the last strength of STF-0 is less than $0.8M_p$ after the fifth cycle (0.045-rad amplitude) but the last strengths of STF-1, STF-2, and STF-3 exceed $0.8M_p$ for all cycles. For the standard W30×99 RBS beam and the W30×99 RBS beam with one pair of stiffeners, local buckling occurred at an amplitude of 0.015 rad. In RBS beams with two or three pairs of stiffeners, local buckling did not occur until the amplitude was raised to 0.030 rad. The last strength of STF-0 is less than $0.8M_p$ after the third cycle (0.030-rad amplitude). The last strength of STF-1 is greater than $0.8M_p$ until the third cycle while the last strengths of STF-2 and STF-3 exceed $0.8M_p$ until the fourth cycle. For the standard W24×76 RBS beam, the last strength was greater than $0.8M_p$ until 0.030 rad of amplitude was applied. However, the RBS beams with one or two pairs of stiffeners sustained $0.8M_p$ of strength until the first cycle at 0.045 rad and the beam with three pairs of stiffeners remained above $0.8M_p$ during the entire loading history.
3. The effect of stiffener thickness on the last strength was small. The stiffener thickness required to provide sufficient strength is the same thickness as the web.
4. The RBS beams with two pairs of stiffeners sustained $0.8M_p$ of strength until the amplitude was raised to 0.030 rad. To withstand an amplitude of 0.045 rad, we recommend using three pairs of stiffeners placed so that they divide the RBS portion into four equal regions.
5. The maximum stress of RBS beams with stiffeners at the fixed end is almost the same as that of the standard RBS beams. On the other hand, the maximum stress of RBS beams with stiffeners in the RBS portion is larger than the maximum stress of standard RBS beams. The maximum stress value of RBS beams with stiffeners is 1.25 times that of standard RBS beams. In addition, the RBS zone is very sensitive and RBS beams with stiffeners can undergo brittle fracture in the welded parts. Full-scale tests are needed to verify the safety of RBS beams with stiffeners.

Acknowledgments

The writers are grateful to Dr. Liu Dawei of Central Research Laboratory, Daiwa House Industry Co., Ltd. for providing helpful information about the numerical analysis. The writers acknowledge Dr. Makoto Muramoto of Kochi National College of Technology for discussing this paper with them.

References

AISC. (2005a). "Seismic provisions for structure steel buildings." *ANSI/AISC 341-5*, Chicago.

AISC. (2005b). "Prequalified connections for special and intermediate steel moment frames for seismic applications." *ANSI/AISC 358-05*, Chicago.

Chi, B., and Uang, C. M. (2002). "Cyclic response and design recom-

mendations reduces beam section moment connections with deep columns." *J. Struct. Eng.*, 128(4), 464–473.

Engelhardt, M. D. (1999). "Design of reduced beam section moment connections." *Proc., Processing North American Steel Construction Conf.*, AISC, Chicago.

Engelhardt, M. D., and Sabol, T. A. (1997). "Seismic-resistant steel moment connections developments since the 1994 Northridge earthquake." *Prog. Struct. Eng. Mater.*, 1(1), 68–77.

Engelhardt, M. D., and Sabol, T. A. (1998). "Reinforcing of steel moment connections with cover plates: Benefits and limitations." *Eng. Struct.*, 20(4–6), 510–520.

Engelhardt, M. D., Winneberger, T., Zekany, A. J., and Potyraj, T. J. (1998). "Experimental investigation of dogbone moment connections." *Eng. J.*, 35(4), 128–139.

FEMA. (2000). "Recommended seismic design criteria for new steel moment-frame buildings." *FEMA 350*, Washington, D.C.

Jones, S. L., Fry, G. T., and Engelhardt, M. D. (2002). "Experimental evaluation of cyclically loaded reduces beam section moment connections." *J. Struct. Eng.*, 128(4), 441–451.

Lee, C. H., Jeon, S. W., Kim, J. H., and Uang, C. M. (2005). "Effects of panel zone strength and beam web connection method on seismic performance of reduced beam section steel moment connections." *J. Struct. Eng.*, 131(12), 1854–1865.

Lee, C. H., and Uang, C. M. (2001). "Analytical modeling and seismic design of steel moment connections with welded straight haunch." *J. Struct. Eng.*, 127(9), 1028–1035.

Nakashima, M., Kanao, I., and Liu, D. (2002). "Lateral instability and lateral bracing of steel beams subjected to cyclic loading." *J. Struct. Eng.*, 128(10), 1308–1316.

Uang, C. M., and Fan, C. C. (2001). "Cyclic stability criteria for steel moment connections with reduced beam section." *J. Struct. Eng.*, 127(9), 1021–1027.

Uang, C. M., Yu, Q. S. K., Noel, S., and Gross, J. (2000). "Cyclic testing of steel moment connections rehabilitated with RBS or welded haunch." *J. Struct. Eng.*, 126(1), 57–68.

Yu, Q. S. K., Uang, C. M., and Gross, J. (2000). "Seismic rehabilitation design of steel moment connection with welded haunch." *J. Struct. Eng.*, 126(1), 69–78.